Soft Matter

Folding of an opened spherical shell†

E. Couturier,*[a] J. Dumais,[b] E. Cerda[a] and E. Katifori[c]

Thin, doubly curved shells occur commonly in nature and their mechanical properties and modes of deformation are very important for engineering structures of all scales. Although there has been substantial work on the stability and modes of failure of thin shells, relatively little work has been done to understand the conditions that promote continuous large scale deformations. A major impediment to progress in this direction is the inherent difficulty in obtaining analytical expressions for the deformed shapes. In this work we propose a new integrable solution which describes the behavior under load of a thin spherical shell with an opening (aperture) of n-fold axial symmetry. We derive a two-parameter family of approximately isometric, constant positive Gaussian curvature shapes that is in excellent agreement with our experimental results of deformed shells (3D scans of compressed ping-pong balls) and simulations (tethered membrane simulations minimizing the stretching and bending energy). The integrable solutions that describe those shapes have n symmetrically arranged curvature singularities which correspond to cusps of the folded shape. We examine the properties of the folded shells and observe that in the analytic solutions isometric closure is more easily achieved when the singularities lie away from the center of the aperture. We find that when allowed by the geometry of the aperture and the nature of the load, physical shells expel the curvature singularities into the aperture.

1 Introduction

Thin, doubly curved shells are common in nature and technology. The stability of man-made shells under various loads as well as their modes of deformation have been extensively studied by engineers for well over a century.[1,2] More recently, research has also focused on the large deformation of soft spherical capsules and colloidosomes in part because of their frequent occurrence in microfluidic systems, nanotechnology, and biology.[3–8] Amidst this extensive research, one aspect of shell mechanics has received relatively little attention – the design of shells to promote flexibility rather than rigidity. One particularly interesting class of flexible shells are those designed to self-seal. This type of shells is beautifully illustrated by pollen grains, a morphologically diverse group of cells found in flowering plants (Fig. 1). The actuation of the pollen grain is both simple and elegant. Most pollen grains are covered by a thin wall which can be subdivided into two regions: the aperture (or apertures) and the inter-apertural regions. The wall over the aperture is typically constituted of cellulose and pectins, two hydrophilic polymers that allow water to diffuse in and out of the cell.[9,10] In contrast,

the inter-apertural wall is impregnated with sporopollenin, a complex biopolymer that stiffens the wall and makes it impermeable to water. When the pollen grain is exposed to air, it rapidly loses water over the aperture leading to a reduction in cell volume. As the pollen desiccates, the surface must deform to accommodate the decreasing volume, a process known as *harmomegathy*.[11] Interestingly, the pollen surface is designed such that the apertural surfaces where water is lost are quickly internalized in the deformation process thus limiting further desiccation and extending the life of the small and vulnerable pollen grain even under harsh environmental conditions (Fig. 1A–D).

The selective pressure for tight self-sealing of the pollen surface is such that pollen grains are unique in their ability to converge reliably to specific folded conformations. The basis for this reliability emerges from the action of the apertures as local soft spots that guide various pollen grains along specific folding pathways.[12] The stereotypical mechanical response of these inhomogeneous shells stands in sharp contrast to the buckling of homogeneous shells, which are notorious for the diversity of equilibrium solutions they achieve even under the simplest loading conditions.[13–16] The same multiplicity of behaviors is also observed in inaperturate pollen grains (Fig. 1E) as they too lack mechanical inhomogeneities to guide their deformation. In contrast to their aperturate counterparts, the surface of inaperturate pollen grains never folds onto itself or provides self-sealing. These pollen grains must use alternative strategies to cope with desiccation and other environmental stresses.[17] The ratio of wall thickness to pollen radius is typically 1/50 or less,

[a]Departamento de Física, Universidad de Santiago de Chile, Santiago, Chile. E-mail: couturier_etienne@yahoo.fr

[b]Facultad de Ingeniería y Ciencias, Universidad Adolfo Ibáñez, Viña del Mar, Chile

[c]Max Planck Institute for Dynamics and Self-Organization (MPIDS), Goettingen, Germany

and the mechanics of the pollen deformation can be approximated as that of a thin shell.

In the design of actuated curved surfaces, the use of spatially variable mechanical properties may be invaluable in providing predictability of deformation and potentially impart novel functions to these systems. With this observation in mind, we have begun a broad study of the mechanical response of inhomogeneous curved shells, using the folding of pollen grains as a source of inspiration.[12] The particular question of interest here is what are the design requirements to achieve self-sealing. The aperture number and pollen geometries are relatively diverse in flowering plants (Fig. 1), suggesting a certain freedom in the design of self-sealing structures.[18] To understand this flexibility, it would be desirable to possess a mathematical framework to analyze the deformation of inhomogeneous shells so as to complement the various modeling approaches already available.

In this article we propose a new analytic approximation to describe the deformation of a thin spherical shell with a star-shaped opening of *n*-fold symmetry. This shape is inspired by the harmomegathic response of the pollen grain of *Dianella caerulea* (Fig. 1B). Our analytic approximation is based on the theory of constant Gaussian curvature surfaces, which can model the inextensional deformation of thin spherical shells. The Gaussian curvature of a surface is the product of the two principal curvatures whereas the mean curvature is the sum of the two principal curvatures. It has been shown that the study of constant Gaussian curvature surfaces (CGC surfaces) is mathematically equivalent to the study of constant mean curvature surfaces[19] which where intensively studied during the 90's.[20] We exploit this duality and adapt tools and ideas from constant mean curvature surfaces to get an integrable family of quasi CGC surfaces (integrable by ODE solving only) that fit well our simulations and experiments of thin shell deformations. The power of this class of solutions is that it is a two-parameter family of surfaces which allows us to explore quickly potential design requirements for the folding of spherical shells.

2 Theory: quasi-isometric deformation of the sphere

Pollen grains, vesicles, colloidosomes, and all other thin-walled shells are physical objects whose mechanical response is dictated by energy considerations. For thin shells, bending modes of deformation (*i.e.* the modes that change the local curvatures of the surface) are known to be energetically less expensive than stretching modes.[21] This result can be understood intuitively by noting that the bending energy scales as $(H/R)^3$, where H is the shell thickness and R is the characteristic size of the shell. On the other hand, the stretching energy scales as (H/R). Accordingly, for a given surface deformation that may involve bending and stretching, the bending energy can be made as small as desired simply by making the shell thinner. We can thus conclude that in a sufficiently thin shell, the deformation will favor bending stresses whenever possible so as to reduce the strain energy. In the limit where the shell thickness tends to zero, we can expect the surface to only bend and not stretch. Such bending-only deformations are known as isometric deformations.

Even in an infinitesimally thin shell, isometric deformations may not always be possible without introducing singular points or lines. The canonical modes of isometric deformation (with singularities) are *mirror reflection* of a segment of the sphere about a dissecting plane and the *folding* of the surface past a meridional slit (Fig. 2). As elegantly shown by Pogorelov,[22] mirror reflection is the geometrical archetype for the buckling response of homogeneous spherical shells. Such snap-through buckling of the sphere is the least energy configuration under a very broad range of loading conditions and shell properties.[13–16] However, no amount of inversion can lead to self-sealing, as can be seen in the inaperturate pollen of *Aristolochia* (Fig. 1E). In contrast, the self-sealing property of aperture pollen grains
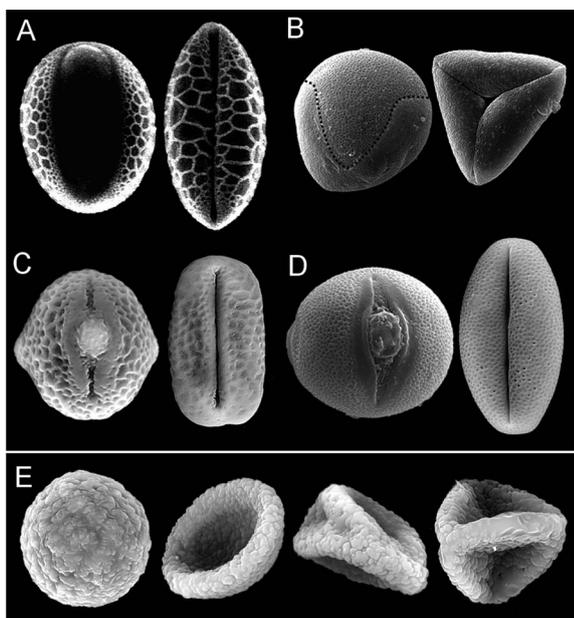

Fig. 1 Harmomegathic response of various pollen grains. (A)–(D) Four examples of aperturate pollen grains showing the hydrated morphology with the aperture exposed (left) and the sealed geometry (right). The pollen grains of *Lilium grandiflorum* (A) and *Dianella caerulea* (B) have a single aperture shown facing the reader; while the pollen grains of *Trifolium repens* (C) and *Euphorbia milii* (D) have three apertures, only one of which is directly visible. (E) The inaperturate pollen grain of *Aristolochia gigantea* illustrates the many configurations that can be realized in the absence of mechanical inhomogeneity, including configurations with one, two, and four major sites of mirror inversion. The characteristic width of the hydrated pollen grains is 30–35 μm except for the much larger *Lilium* pollen which reaches 100 μm. For ease of view, the aperture margin in (B) (hydrated state of *Dianella*) has been marked with a dashed black line.
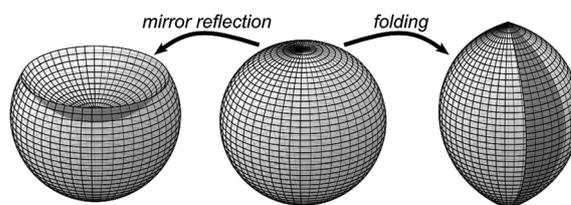

Fig. 2 Two canonical isometric deformations of the sphere. Mirror reflection leads to rapid reduction of volume but the entire surface of the sphere remains exposed. In contrast, a folding sphere accommodates the reduction in volume by internalizing the excess surface area.

(Fig. 1A–D) is closely approximated by the folding of the sphere (Fig. 2). Studies of this mode of deformation are much more scarce and therefore there is only limited information about the conditions that promote it.[12]

We posit that self-sealing in a shell is promoted, as in apperturate pollen grains, by mechanical inhomogeneities. The mechanical response of a closed shell with a soft sector can be approximated as that of an open shell when the Young's modulus of the soft sector becomes infinitesimally small. Thus, the deformations of open shells can be a good approximation of inhomogeneous closed shells, such as pollen grains. We therefore seek a set of isometric solutions for the deformation of an open sphere. The problem is daunting and despite decades of mathematical research on isometric deformations of surfaces, few concrete solutions are available. Two notable cases are the infinitesimal deformation of the sphere[23,24] and the so-called Smyth surface.[25] Unfortunately, neither of those solutions offers a convincing fit of the observed deformation of aperturate pollen grains.

When studying isometric deformations, the common practice is to describe surfaces in terms of two fundamental forms I and II:

$$I = E du^2 + 2F du dv + G dv^2 \qquad (1)$$

$$II = L du^2 + 2M du dv + N dv^2 \qquad (2)$$

where u and v are curvilinear coordinates on the surface and the coefficients (E, F, *etc.*) verify a set of compatibility equations (the two Codazzi equations and the Gauss equation). The two fundamental forms serve to define the metric properties of the surface and the principal curvatures. They correspond to a system of ordinary differential equations whose solution is the surface.

Gauss' *teorema egregium* states that the Gaussian curvature can be expressed with only the coefficients of the metric. As a consequence the Gaussian curvature is invariant under isometric deformations. However, the converse is not necessarily true, *i.e.* a deformation that preserves the Gaussian curvature is not necessarily isometric (imagine for example, displacing points on the surface of the sphere. The Gaussian curvature remains constant but the metric is changed). Nevertheless as stated by the Minding's theorem (1839)[26] all surfaces with the same constant curvature K are locally isometric.

In the particular case of constant Gaussian curvature surfaces (CGC surfaces), the two fundamental forms can be written such that the two Codazzi equations are automatically satisfied.[27] We can further change the system of coordinates from (u, v) to (ρ, θ) where $z = u + iv = \rho e^{i\theta}$ and rewrite the system of equations so that the derivation of the surface morphology reduces to determining two functions: $\omega(\rho, \theta)$ and a holomorphic function $\phi(z)$. Finally, we can impose the *n*-fold symmetry of the surface by setting $\omega(\rho, \theta) \to \omega(\rho, n\theta)$[25] (see the ESI† for the derivation). With these assumptions, the Gauss compatibility equation can be written as

$$\Delta\omega + (e^{2\omega} - \lambda\rho^{2(n-2)}e^{-2\omega}) = 0 \qquad (3)$$

and the function ω can be determined which leads to the two fundamental forms. The coefficient λ is a free parameter that controls the amount of deformation. When $\lambda = 0$ which corresponds to the sphere, eqn (3) is called the Liouville equation. After the above transformation, the parameters of the two fundamental forms are

$$E = \frac{-2\lambda\rho^{n-2}\cos(n\theta) + e^{2\omega} + \lambda^2\rho^{2(n-2)}e^{-2\omega}}{K}$$

$$F = \frac{2\lambda\rho^{n-1}\sin(n\theta)}{K}$$

$$G = \frac{2\lambda\rho^n\cos(n\theta) + \rho^2\left(e^{2\omega} + \lambda^2\rho^{2(n-2)}e^{-2\omega}\right)}{K}$$

$$L = \frac{\left(e^{2\omega} - \lambda^2\rho^{2(n-2)}e^{-2\omega}\right)}{\sqrt{K}}$$

$$M = 0$$

$$N = \frac{\rho^2\left(e^{2\omega} - \lambda^2\rho^{2(n-2)}e^{-2\omega}\right)}{\sqrt{K}} \qquad (4)$$

Without loss of generality, unless otherwise stated, in this article we set the Gaussian curvature to $K = 1$ and the symmetry to $n = 3$.

One particular integrable solution of CGC surfaces with symmetry $n = 3$ is the Smyth surface.[25] It uses solutions of eqn (3) that are independent of the variable θ. Although the solution has a $n = 3$ symmetry like the pollen of *Dianella* and the geometry we seek in our experiments (Fig. 3), this family of surfaces only adequately describes the behavior of a small part of the deformed sphere below the aperture. Here, instead of seeking a strictly isometric family of solutions, we allow the Gaussian curvature to have minor deviations from the desired $K = 1$ and obtain a family of surfaces that predicts the overall deformed shell shape, such as the deformed ping-pong ball, much more successfully than the Smyth surface. We call these surfaces quasi-CGC surfaces.

There is no known exact analytical family of solution which fulfills continuously the Liouville equation and the sinh-Gordon equation.[28] To approximate the analytically intractable full sinh-Gordon equation,[3] we discard the term $\lambda\rho^{2(n-2)}e^{-2\omega}$ which leads to a fully integrable Liouville equation:

$$\Delta\omega + e^{2\omega} = 0 \qquad (5)$$

This reduced equation is equivalent to the Gauss equation for the sphere; but, unlike the Gauss equation, eqn (5) can be solved analytically. This approximation is accurate sufficiently close to the umbilic point (small ρ) at the lower pole of the sphere and for a small value of λ.
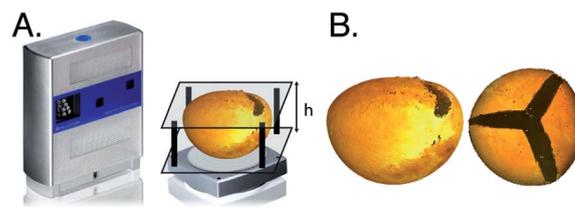

Fig. 3 Experiment of compression of a ping-pong ball. (A) Experimental set-up with a scanner and a compressed ping-pong ball. (B) Side view and top view of the dissected ping-pong ball in the compressed state.

We propose a function $\omega(\mu, z)$ which satisfies eqn (5) and has a n-fold symmetry in θ:

$$\omega = \log \frac{2\mu|(1 + (n-1)z^n)|}{|(1-z^n)|^2 + \mu^2|z|^2} \tag{6}$$

where $z = \rho e^{i\theta}$ and μ is a parameter controlling the geometry of the surface. Substituting ω in eqn (4) leads to pseudo-fundamental forms and to a pseudo-Bonnet system.[26] We integrate this system along the ρ coordinate with initial conditions detailed in the ESI.† This integration leads to a two-parameter (λ, μ) family of surfaces whose Gaussian curvature K stays roughly constant even at large deformations (see ESI†).

A formal justification of the approximation eqn (5) is not obvious due to the nonlinearity of the partial differential equations and the successive step of integration. Nevertheless we observe that the Gaussian curvature oscillates sufficiently close to the target value and this family of surfaces is in remarkable agreement with the results of our experiments and simulations, detailed in Materials and methods. In addition, the family of quasi CGC surfaces that we find using eqn (6) is not unique. However, this family is able to predict very well the shapes from deformations resulting from two very different boundary conditions, (one examined by experiment and one by simulation), pointing to the generality and usefulness of the integrable solutions we found. In fact, other loads on the shells could lead to different families of isometric deformations.

3 Material and methods

3.1 Shell deformation experiments

Direct experimental analysis of folding pollen grains is difficult technically because of the small size of these structures and also because their hydrated geometry often deviates sharply from that of a sphere. To gain some physical appreciation for the deformation of open shells under load, we worked instead with ping-pong balls. The diameter of the balls was 39.7 ± 0.05 mm and the wall thickness was 0.38 ± 0.02 mm. According to the literature, the Young modulus is between 3.2 and 4.8 GPa.[29] Part of the ping-pong ball was cut off to create an opening resembling the three-fold axial symmetry of the *Dianella* pollen grain aperture (see ESI† for detail). The ball was positioned between two glass slides so that its axis of symmetry was perpendicular to the slides. We varied the compression, as imposed by the ping-pong ball confinement between the two parallel slides positioned at distance h. We measured the shape of the surface at each compression h using a NextEngine 3D scanner (Fig. 3A) with the associated NextEngineHD Scan software for the surface reconstruction (Fig. 3B). The mesh computed with the NextEngineHD Scan software was imported in Matlab (The MathWorks, Natick, MA, USA) for fitting with splines and for the computation of curvatures and lengths. As a control, we placed an uncut and uncompressed ping-pong ball between identical glass slides and recovered the radius of curvature up to 0.5%.

3.2 Simulations

To study computationally the deformation pathways of aperturate shells with n-fold axial symmetry, we performed tethered membrane simulations following the protocol refined by (ref. 12) and first introduced by (ref. 30). The shell is approximated by a tessellated mesh that can be regular or randomized. The mesh links are treated as hookean springs that determine the stretching energy of the deformation

$$E_{\mathrm{str}}(\{\vec{r}\}) = \frac{1}{2}\varepsilon \sum_{\langle ij \rangle}\left(|\vec{r}_i - \vec{r}_j| - \rho_{ij}\right)^2 \tag{7}$$

where $\vec{r}_i$ are the coordinates of point i, the sum is over the mesh bonds connecting pairs of points (i, j), ρ_{ij} is the rest length of the bond ij and ε is the discretized stretching modulus. The bending energy of the shell depends on the angle ϕ_{mk} between each pair (m, k) of contiguous facets:

$$E_{\mathrm{bend}}(\{\vec{r}\}) = -\frac{1}{2}\kappa \sum_{\langle mk \rangle}\cos(\phi_{mk} - \phi_{mk}^0) \tag{8}$$

where ϕ_{mk}^0 is the rest angle at zero deformation and κ is the discretized bending modulus. These parameters specifying the mechanical properties of the shell were chosen to match those of a thin spherical shell (ratio of thickness to radius $H/R < 1/100$) and the ping-pong ball. In particular, the spontaneous curvature, as implemented by the angle ϕ_{mk}^0 was $1/R$, where R is the radius of the sphere, and ρ_{ij} was chosen so that the zero load shape is strain free. The other relevant parameter is the ratio κ/ε, which depends on the thickness of the sphere. We chose a value of the same order as that of the ping-pong ball, namely $H/R = 1/300$. Details of the choice of the mesh and the corresponding discretized energy equations are given in the ESI.†

The apertures of the shells are composed of n identical, wedge-shaped units, each rotated by an angle of $2\pi/n$. The aperture was first drawn in the plane using the same function $(x(\theta), y(\theta))$ for each of the repeating units:

$$x(\theta) = a_{\mathrm{s}}[\cos(n\theta)^{m_{\mathrm{s}}}\cos(\theta) - x_{\mathrm{o}}] \tag{9}$$

$$y(\theta) = a_{\mathrm{s}}[\cos(n\theta)^{m_{\mathrm{s}}}\sin(\theta)] \tag{10}$$

where $|\theta|$ varies between θ_0 and $\pi/(2n)$, the parameters m_{s} and x_{o} determine the sharpness of the aperture wedge, and a_{s} sets its size. The cutoff θ_{o} corresponds to the intersection point of two segments rotated by $2\pi/n$, the concave corners of the aperture (see ESI† for details). The angle at the tip of the wedge, the convex corner, termed "aperture corner", or just "corner" in the text depends on the parameters $(m_{\mathrm{s}}, x_{\mathrm{o}})$. To associate the planar image of the aperture with the vertices on the tethered spherical mesh, the latter was stereographically projected onto a plane, and the mesh points whose projection fell within the aperture outline were removed from the tessellation.

To explore the effect of aperture geometry on the folding pathway, we used nine different aperture shapes that combined three levels of sharpness set by $(m_{\mathrm{s}}, x_{\mathrm{o}})$ and three sizes a_{s} such that the tip of the aperture wedge was above, below or at the sphere equator (see ESI†). In the text, we denote these shapes by α, β and γ (α being the sharpest and γ being the widest), subscripted by 1, 2 and 3 for apertures above the equator, at the equator, or below the equator, respectively.

Two loads were used to actuate the deformation of the shell. In the first case, an effective attractive hookean potential was

applied between the three points that came nearest to the upper pole of the sphere. The second approach was to apply a repulsive potential between the three points on the shell opening that were farthest away from the upper pole (*i.e.* the three aperture corners in the shell):

$$V(\{\vec{x}\}, a_r) = \sum_{\langle kl \rangle} \frac{1}{2} \left(|\vec{x}_k - \vec{x}_l| - (1 - a_r) x_{kl}^0 \right)^2. \quad (11)$$

where $\vec{x}_k$ are the coordinates of the k corner and x_{kl}^0 is the distance at zero deformation of the (kl) corner pair. The parameter a_r is positive in the case of an effective attractive potential and negative in the case of a repulsive potential, and its magnitude determines the extent of the deformation load. The mesh point coordinates are determined for each load by minimizing the sum of the stretching E_{str}, bending E_{bend} and load energy $V(\{\vec{x}\}, a_r)$ using a conjugate gradient minimization routine.

4 Results and discussion

4.1 Quasi-isometric deformation of the sphere

We begin with a parametric analysis of the solutions outlined in Section 2 (Fig. 4). Two parameters characterize this family of surfaces. The parameter μ determines the geodesic coordinates of the three singularities. These singularities are the $n = 3$ cusp like points on the surface where the solution is not differentiable and the curvatures cannot be defined. At small μ, the singularities lie near the lower pole of the sphere while for large μ they lie near the top. In contrast, the parameter λ determines the amount of bending, where $\lambda = 0$ corresponds to the sphere.

To assess the ability of this family of solutions to maintain a constant Gaussian curvature K, we computed the principal curvatures of the surface (see ESI†). For the range of μ values represented in Fig. 4, the Gaussian curvature on the whole surface remains constant up to a deformation (reduction of the height h) of 15–25%, with the upper range observed for smaller values of μ. For example, the shells obtained for $\lambda = 6$ in Fig. 4

conserve K everywhere for small μ, but not for higher μ (in particular for $\mu \gtrsim 2.5$). Therefore, shell closure at constant Gaussian curvature is more easily achieved for singularities lying low on the sphere (small μ values). Accordingly, we can conclude that apertures spanning a large meridional region of a spherical shell are better suited for closure *via* low energy bending modes.

4.2 Comparison of analytic solution with experiments and simulations

The reconstructed geometry of the ping-pong ball deformed between two parallel plates is illustrated in Fig. 5A. As expected, considering the thickness of the shell, the deformation was mainly due to bending and not stretching. Due to the contact of the ping-pong ball with the glass slide at the very bottom and the resulting local compression, there was some deformation. The maximum length change for the longest meridian was less than 4% (Fig. 5C). This 4% variation is an upper bound: it is due to both the deformation induced by mechanics and the computational reconstruction of the 3D shape, especially the "gluing" of different faces by the software of the 3D scanner. The fluctuations in the Gaussian curvature were below the precision of our measurements (about 5%). In contrast, the square of the mean curvature, which has the same units as the Gaussian curvature, showed a variation as large as 22%. Therefore, although the deformation caused large changes in individual curvatures, it did not affect significantly the Gaussian curvature. Fig. 5B shows the results of a tethered mesh simulation with attractive potential at the tip of the shell. The deformation was almost perfectly isometric with the stretching
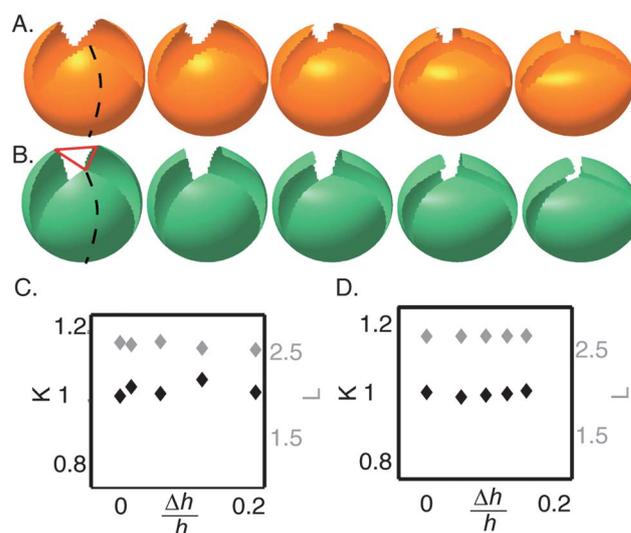
Fig. 5 Deformation of a sphere with a 3-fold axially symmetric aperture. (A) 3D scan of a ping-pong ball compressed between two parallel plates. (B) Tethered mesh simulation of the deformation of a sphere with a 3-fold aperture. Closure was driven by "stitching" the three extremities at the top (represented by three red lines in the left panel). (C) Length of the longest geodesic (L) and Gaussian curvature K as a function of the relative compression ($\Delta h/h$). The length varies by approximately 4% during the deformation. The change in Gaussian curvature in the experiments is below the resolution of the reconstructions. (D) The same parameters as in (C) but measured on the tethered mesh simulations. The length change is $\ll$0.1% for the entire deformation.
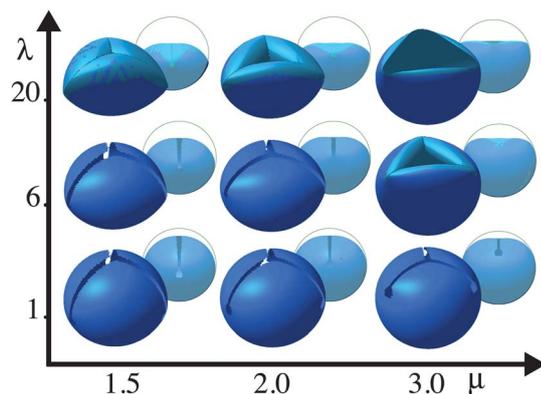

Fig. 4 A two-parameter family of quasi-CGC surfaces. The geodesic distance between the singularities and the lower pole increases with μ while the deformation increases with λ ($\lambda = 0$ is a sphere). Dark and light blue regions indicate where the Gaussian curvature deviates from $K = 1$ by less than 5% and more than 5%, respectively. At large μ and λ, the solution becomes singular and thus cannot be continued to close the surface. Insets show lateral views for each of the surfaces, and their deviation from a circular (undeformed) cross-section.

remaining well below 0.1% (Fig. 5B and D). Interestingly, this family of surfaces is similar to the one obtained in the ping-pong ball experiments (Fig. 5A and C), where the load was applied by vertical confinement of the ball.

We next turn to a comparison of these experimental and simulation surfaces with the integrable solutions for quasi-CGC surfaces. We first note that the deformation of these shells does not correspond to a simple increase of λ with a constant μ. The real surfaces of the successive deformations are regions of quasi-CGC surfaces with different λ and μ. In other words, the deformation of the ping-pong ball is not necessarily represented by a simple path in parameter space of the quasi-CGC. A priori, it would be appealing to predict the different experimental and simulation results by finding the quasi-CGC surface that satisfies the same boundary conditions and minimizes the strain energy. However, such an approach is impossible because we do not have an explicit map of material points between the sphere and the deformed quasi-CGC, which would allow us to compute the in-plane strains that must inevitably exist since the solutions are not strictly isometric. Without a proper assessment of the stretching energy, minimization of the bending energy is futile.[31] Instead of using energy minimization to predict specific shell geometries, we use a best-fit approach among our family of surfaces (see ESI† for details).

The integrable solutions provide a very good fit both for the experiments and simulations (Fig. 6 and 7). The fit obtained with experiments was very good given the difficulty associated with the preparation of a symmetric shell by hand. In fact, where the Gaussian curvature of the CGC surfaces deviates significantly from a constant (that of the initial spherical shape), the deviations between experimental and theoretical results can be attributed primarily to the geometrical approximations, since both the simulations and the experiments are to a large degree (as measured) inextensional.

In Fig. 6A and B we compare the experimental surface, obtained by compression of a ping-pong ball, with the analytical
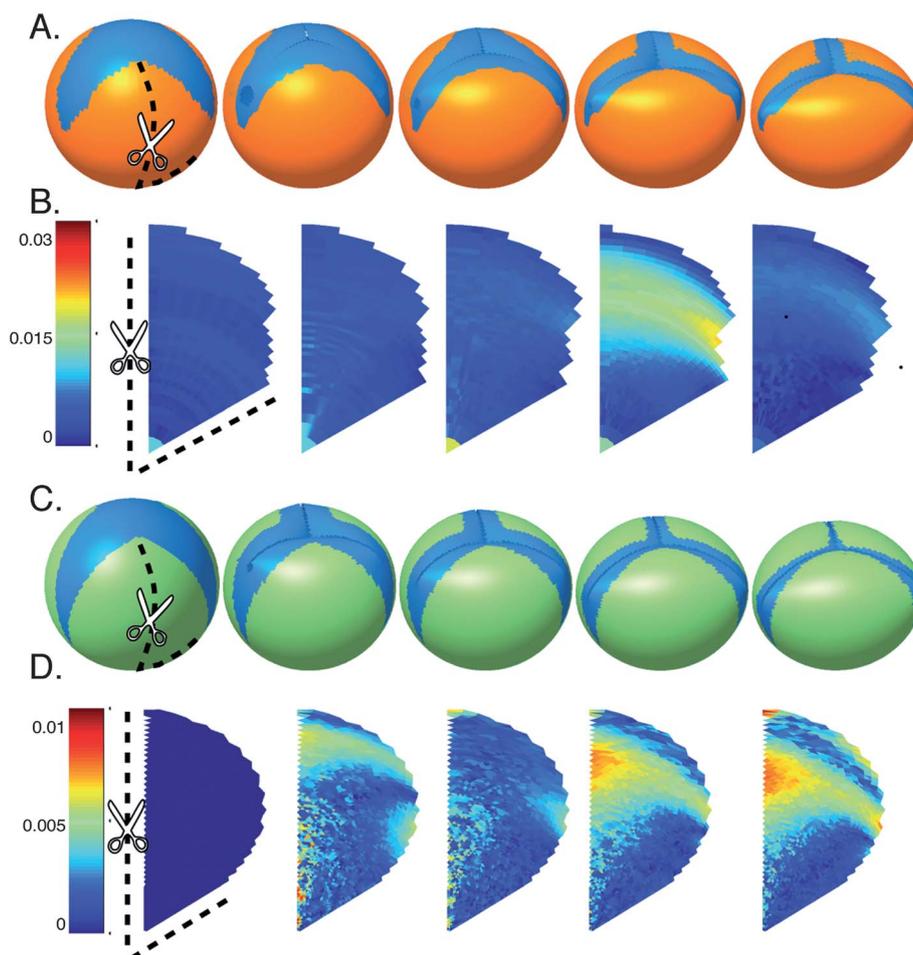

Fig. 6 Comparison of the analytic surface with experiments and simulations. The μ and λ of the analytic solution at each stage of the deformation were chosen so that the analytic solution fits best the experimentally or computationally obtained surface. (A) Quasi-CGC surfaces that best fit the deformation pathway of a compressed ping-pong ball (orange). The aperture of the ping-pong shell, projected on the deformed shape (blue). Each experimental (and analytic) shell can be decomposed in six sectors that are either identical or mirrors of each other, as marked by the dashed line and scissors. (B) Euclidean distance between one of these sectors of the deformed ping-pong ball and the best fit quasi-CGC surface plotted in spherical coordinates. (C) Quasi-CGC surfaces that best fit the deformation pathway of a simulation with aperture shape α_3 (green). The aperture of the α_3 shell, projected on the deformed shape (blue). (D) Euclidean distance between one of the sectors of the deformed simulation shell and the best fit quasi-CGC surface plotted in spherical coordinates. Numbers on the color bar are in units of the diameter of the undeformed sphere.

surface that best fits the experiment. To determine the parameters $(\tilde{\mu}, \tilde{\lambda})$ that produce a quasi-CGC surface $P_{(\tilde{\mu}, \tilde{\lambda})}$ that best fits the computationally or experimentally obtained shape S, we calculated the maximal distance $d(S, (\mu, \lambda))$ of S to each surface in the set $\{P\}$ (distance of point of S that is the furthest away from any point in $P_{(\mu, \lambda)}$, when S and $P_{(\mu, \lambda)}$ are matched at the umbilical point). Finally, we chose $P_{(\tilde{\mu}, \tilde{\lambda})}$ that had the minimum $d(S, (\mu, \lambda))$. We projected the aperture of the surface S to a large set of surfaces $\{P\}$ produced by scanning a large number of parameters (μ, λ), and excised the points inside the projected aperture. Further details about the best fit are presented in the ESI.†

In Fig. 6A we plot the deformation pathway of the best fit quasi-CGC surface and in Fig. 6B we plot the distance map (point to point distance) between the two surfaces. As can be seen from the values on the colorbar, we reach a precision of 2% for the entire deformation.

The comparison with the simulations was performed for a great variety of apertures. An example is shown in Fig. 6C and D. For short apertures, we could fit the surface with a precision of at least 1% of the diameter until a decrease of the compression height h by 8%. For longer apertures, we could reach a 20% decrease of the height while staying below this threshold (Fig. 6C and D and ESI†).

The first observation from the comparison between the experimental or the computational surface and the best fit quasi-CGC surface is that the singularities of the analytically derived shape do not coincide with the aperture corners of the experimental or simulation surfaces, but typically lie inside the projected aperture.

The integrable approximation we develop in this work provides a closed formula for the three lines of the surface (cross-sections of the shell) which are situated in its three planes of symmetry[32] (see ESI† for details of the calculation). An example is presented in Fig. 7. In Fig. 7A, we show simulation α_3 and the best analytic fit. The shaded plane represents the orientation of the plane of symmetry of the shell. In Fig. 7B we present the cross-section of a compressed ping-pong ball at successive stages of deformation, as determined by experimental measurements with the 3D scanner (empty circles). The solid line is the best fit among the quasi-CGC surfaces, and the asterisks are the singularity of the quasi-CGC prediction. The two-parameter analytic solution in closed form provides an excellent fit to the experimental data. Note that the analytic solution is independent of the
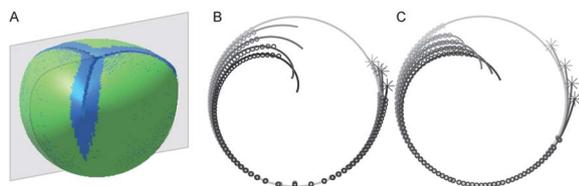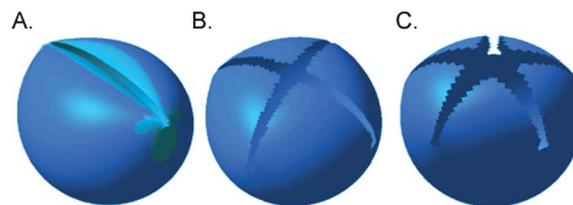

Fig. 8 Quasi-CGC surfaces with symmetry 2 (A), 4 (B), and 5 (C). The light blue color corresponds to the global surface obtained for a given λ and μ. The dark blue color corresponds to the part of the surface which has a Gaussian curvature differing from $K = 1$ by less than 5%.

nature of the load that actuates the deformation. For that reason, the fit deviates slightly at the top of the surface. In Fig. 7C we show the cross-section of a "stitched" simulation result (empty circles). The solid line is the best fit among the quasi-CGC surfaces. The two-parameter analytic solution in closed form again provides an excellent fit to the computational data.

4.3 The role of the symmetry in shell folding

We have also explored the role of symmetry on the ability of a shell to self-seal. In addition to $n = 3$, we calculated the analytic shape and simulation results for $n = 2, 4, 5$ and 6. The response of these surfaces to changes in λ and μ is qualitatively similar to the $n = 3$ case. Examples of the analytic solution are shown in Fig. 8. A notable case is the symmetry $n = 2$ solution. In this case, in contrast to the analytic axisymmetric solution discussed in (ref. 12) and presented in Fig. 2, the surface bends inwards close to the aperture margins. This is in good agreement with experimental observations of aperturate pollen grains (e.g. in Fig. 1A) and other experimental systems and simulations.[12] Although in these examples the aperture is defined by a low Young modulus, rather than a completely removed sector, we can speculate that part of the curvature of the shell near the aperture is due to geometrical reasons and not due to the invagination of the aperture material.
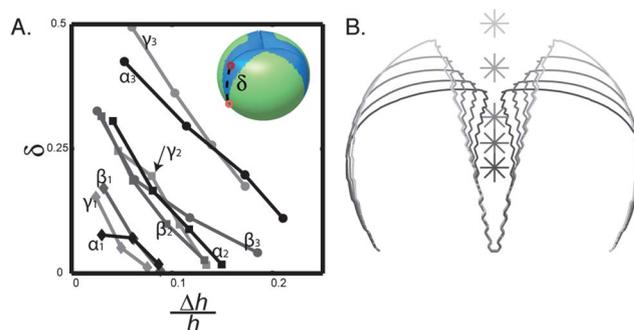

Fig. 9 The singularity gets closer to the corner as the compression increases. (A) The distance δ between the corner (orange ○) of the simulation and the singularity (red ○) of the best fitting quasi-CGC surface decreases when the deformation increases. The symbols and line colors denote the simulations of the different aperture shapes. (◆) black: α_1, (■) black: α_2, (●) black: α_3, (◆) dark gray: β_1, (■) dark gray: β_2, (●) dark gray: β_3, (◆) light gray: γ_1, (■) light gray: γ_2, and (●) light gray: γ_3. (B) One of the three angles of the aperture is superimposed at the successive deformation stages to show its invariance. The star corresponds to the singularity of the quasi CGC best fit surface. The simulation represented here is the simulation α_3.

Fig. 7 Analytic fit of the shape of the profile in the plane of symmetry. (A): plane of symmetry (orientation of the cross-sectional plane). (B) ○: experimental measurement of the profile of a compressed ping-pong ball. Solid line: best fit among the quasi-CGC surfaces. *: singularity of the quasi-CGC prediction. (C) ○: profile of simulation α_3 triggered by stitching of the top (same as Fig. 6). Solid line: best fit among the quasi-CGC surfaces.

4.4 Position of the singularities

Another remarkable property of this fit is that when the deformation increases, the corner of the shell surface gets closer to the singularity of the quasi-CGC surface that best fits the overall surface (Fig. 9A). No stretching appears at the corner until the conclusion of the deformation. As the deformation at the aperture corner remains isometric, the angle of the aperture rim at the corner remains constant while the singularity moves. The successive angles at the corner can be perfectly superimposed (Fig. 9B) (see also ESI† Fig. S6). The corner typically never closes during the deformation.

5   Conclusions

In this work we have derived a two-parameter quasi constant Gaussian curvature family of surfaces with n-fold symmetry of rotation, and shown that these surfaces are in excellent agreement with both experiments and simulations. The two parameters that control the shape of the surfaces of this family qualitatively correspond to the position of the singularities and the amount of deformation. This family of quasi-isometric surfaces can provide intuition on how to design aperturate foldable structures that successfully close and seal the aperture. Concordance between the quasi-isometric deformations and the experimental deformation of shells requires that the latter be thin. Thick shells cannot be successfully approximated with CGC surfaces because both bending and stretching come into play in such shells.
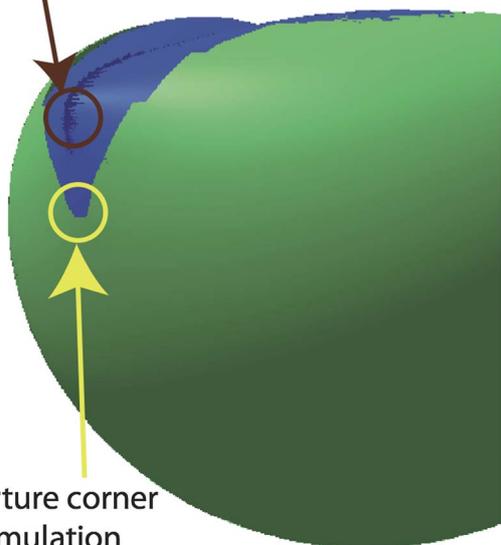

Fig. 10 The aperture corner wraps around the singularity. Green: simulation of the folded shell. Blue: the best fit quasi-CGC surface. The quasi-CGC surface is placed inside the simulation to visualize the relative position of the singularity and the aperture.

Isometric deformations are ideal for closing the sphere because they are low energy modes. However, using isometric deformations to model a self sealing structure can lead to an apparent contradiction. With a purely isometric deformation, none of the angles in the plane of the shell can change; this includes also the angle in the aperture corners. Therefore, as the flaps of the shell meet together to close the center of the aperture, they leave openings at the corners. We are therefore left with a paradox: isometric modes can promote large deformations at low energetic cost to close an aperture but at the same time they preclude closing at the aperture corners. This paradox is resolved by bringing the "conical" singularity deep into the aperture corner. The surface of the shell can wrap around this singularity leaving an increasingly small opening in the shell (Fig. 10). This, however, is done at a high energy cost because the individual curvatures diverge at this point. It is for this reason that bending and stretching energy often mix at these locations.

The geometry adopted by the spherical shells just studied is one where the curvature singularities typically lie within the aperture so that the infinite curvature reached at those points does not contribute to the elastic energy of the folded shape. For increasing deformation (*i.e.* the principal curvatures depart from $1/R$, where R is the radius of the shell) the singularities gradually approach the boundary of the "physical" shell.

This observation emphasizes a shortcoming of the simple axisymmetric solution that was put forward previously to describe the Lily pollen grains.[12] The axisymmetric constant Gaussian curvature surface disagrees with our observation that the angle of the aperture corner preferably remains constant during the isometric deformation. The class of axisymmetric CGC surfaces develops a singularity at the boundary of the domain as soon as the deformation begins. For this reason, this axisymmetric inextensional solution is particularly unfavorable compared to the quasi-CGC surfaces we introduce in this work. An optimal self-sealing shape should delay the formation of a cusp at the corner until the very last stages of the sealing. In fact, this is what is observed in pollen grains. Pollen grain apertures have rounded corners which typically remain slightly open once the shell is closed. Perfect geometric sealing of the grain is not necessary to substantially delay dehydration.

Depending on the possible design constraints of the aperture (*e.g.* position and sharpness of the corners and apertural area), our two-parameter family of surfaces can help determine the foldability of engineering structures and identify potential problems. For example, the corner angle conservation and the fact that the aperture corners will tend to "wrap around" the singularities point to the fact that the corners are points that require some engineering innovation in the foldable shell design choices. Similarly, apertures with corners above the equator might pose a challenge. Pollen grains can provide inspiration on how to overcome issues such as these.

From a mathematical point of view, our approximation gives a sparse representation of the sphere deformation: despite the diversity of boundary conditions in the stitching simulation, the deformed shapes can be accurately described by our two-parameter surface family (μ, λ). For other boundary conditions, such as deformations actuated by repulsion of the corners, in

several instances the surface can be partially described by our family of surfaces, which provide a good fit only for the bottom of the structure. Finding the corresponding ω function for these cases remains an open question.

More generally it would be interesting to link approximation to other more sophisticated methods which generate constant mean curvature surfaces.[33] As the equations determining a constant Gaussian curvature surface are the same as the ones for constant mean curvature surfaces, this method could be used in capillarity questions, to describe the interface between two fluids with different pressures separated by a soap film, for boundary conditions similar to the ones of this article.

Acknowledgements

References

1 A. E. H. Love, *A Treatise on the Mathematical Theory of Elasticity*, Cambridge University Press, 1927.

2 S. Fluegge, *Stresses in shells*, Springer-Verlag, 1960.

3 C. Quilliet, Depressions at the surface of an elastic spherical shell submitted to external pressure, *Phys. Rev. E: Stat., Nonlinear, Soft Matter Phys.*, October 2006, **74**, 046608.

4 N. Tsapis, E. Dufresne, S. Sinha, C. Riera, J. Hutchinson, L. Mahadevan and D. Weitz, Onset of Buckling in Drying Droplets of Colloidal Suspensions, *Phys. Rev. Lett.*, January 2005, **94**, 018302.

5 C. Quilliet, C. Zoldesi, C. Riera, A. van Blaaderen and A. Imhof, Anisotropic colloids through non-trivial buckling, *Eur. Phys. J. E: Soft Matter Biol. Phys.*, 2008, **27**(no. 1), 13–20.

6 S. S. Datta, H. C. Shum and D. A. Weitz, Controlled Buckling and Crumpling of Nanoparticle-Coated Droplets, *Langmuir*, December 2010, **26**, 18612–18616.

7 S. Datta, S.-H. Kim, J. Paulose, A. Abbaspourrad, D. Nelson and D. Weitz, Delayed Buckling and Guided Folding of Inhomogeneous Capsules, *Phys. Rev. Lett.*, September 2012, **109**, 134302.

8 J. Paulose, G. A. Vliegenthart, G. Gompper and D. R. Nelson, Fluctuating shells under pressure, *Proc. Natl. Acad. Sci. U. S. A.*, 2012, **109**(no. 48), 19551–19556.

9 J. Heslop-Harrison, Pollen walls as adaptive systems, *Ann. Mo. Bot. Gard.*, 1979, **66**(no. 4), 813–829.

10 J. Heslop-Harrison, An interpretation of the hydrodynamics of pollen, *Am. J. Bot.*, 1979, **66**(no. 6), 737–743.

11 R. P. Wodehouse, *Pollen grains*, Mc Graw-Hill, London, 1935.

12 E. Katifori, S. Alben, E. Cerda, D. R. Nelson and J. Dumais, Foldable structures and the natural design of pollen grains, *Proc. Natl. Acad. Sci. U. S. A.*, April 2010, **107**, 7635–7639.

13 L. Pauchard and S. Rica, Contact and compression of elastic spherical shells: The physics of a 'ping-pong' ball, *Philos. Mag. B*, August 1998, **78**, 225–233.

14 X. L. Dong, Z. Y. Gao and T. X. Yu, Dynamic crushing of thin-walled spheres: An experimental study, *Int. J. Impact Eng.*, August 2008, **35**, 717–726.

15 C. Quilliet, Numerical deflation of beach balls with various Poisson's ratios: From sphere to bowl's shape, *Eur. Phys. J. E: Soft Matter Biol. Phys.*, June 2012, **35**, 48.

16 A. Vaziri and L. Mahadevan, Localized and extended deformations of elastic shells, *Proc. Natl. Acad. Sci. U. S. A.*, 2008, **105**(no. 23), 7913–7918.

17 N. Firon, M. Nepi and E. Pacini, Water status and associated processes mark critical stages in pollen development and functioning, *Ann. Bot.*, May 2012, **109**, 1201–1213.

18 H. Halbritter and M. Hesse, Principal modes of infoldings in tricolp(or)ate Angiosperm pollen, *Grana*, March 2004, **43**, 1–14.

19 G. Darboux, *Leçons sur la théorie générale des surfaces*, Gauthiers-Villars, 1896.

20 K. Kenmotsu, Surfaces With Constant Mean Curvature, *Translations of Mathematical Monographs*, American Mathematical Society, 2003.

21 L. D. Landau and E. M. Lifshitz, *Theory of Elasticity*, Pergamon Press, 1986.

22 A. V. Pogorelov, *Bendings of Surfaces and Stability of Shells*, American Mathematical Society, 1988.

23 D. D. Bleecker, Infinitesimal Deformations of Portions of the Standard Sphere in E3, *The American Mathematical Monthly*, 1980, **87**, 175–182.

24 A. V. Pogorelov, *Extrinsic Geometry of Convex Surfaces*, American Mathematical Soc., 1973, vol. 35.

25 B. Smyth, A Generalization of a Theorem of Delaunay on Constant Mean Curvature Surfaces, in *The IMA Volumes in Mathematics and its Applications*, NY: Springer, New York, 1993, pp. 123–130.

26 M. Spivak, *A comprehensive introduction to differential geometry*, Publish or perish, 1979, vol. 5.

27 T. Klotz, Some Uses of the Second Conformal Structure on Strictly Convex Surfaces, *Proc. Am. Math. Soc.*, 1963, **14**(no. 5), 793–799.

28 T. Dauxois, S. Fauve and L. Tuckerman, Stability of periodic arrays of vortices, *Phys. Fluids*, 1996, **8**(no. 2), 487.

29 H. H. Ruan, Z. Y. Gao and T. X. Yu, Crushing of thin-walled spheres and sphere arrays, *Int. J. Mech. Sci.*, February 2006, **48**, 117–133.

30 H. Seung and D. Nelson, Defects in flexible membranes with crystalline order, *Phys. Rev. A: At., Mol., Opt. Phys.*, July 1988, **38**, 1005–1018.

31 C. D. Santangelo, Nambu–Goldstone modes and diffuse deformations in elastic shells, *Soft Matter*, 2013, DOI: 10.1039/C3SM50476J.

32 R. Walter, Explicit examples to the H-problem of heinz hopf, *Geom Dedicata*, June 1987, **23**, 187–213.

33 S. Fujimori, S. Kobayashi and W. Rossman, Loop Group Methods for Constant Mean Curvature Surfaces, *Rokko Lectures in Mathematics*, 2005.